Polyamorphism and density anomalies in network-forming fluids: Zeroth- and first-order approximations

C. J. Roberts and Pablo G. Debenedetti[a)]
Department of Chemical Engineering, Princeton University, Princeton, New Jersey 08544

(Received 20 February 1996; accepted 4 April 1996)

A molecular model of network-forming liquids has been formulated in terms of a lattice fluid in which bond formation depends strongly on molecular orientations and *local* density. The model has been solved in the zeroth- and first-order approximations for molecular and bond geometries similar to water or silica. Results are presented in the form of fluid-phase boundaries, limits of stability, and loci of density extrema. At low temperatures and high pressures the first-order solution shows a liquid–liquid transition with upper and lower consolute temperatures, in addition to vapor–liquid equilibrium; and two loci of density extrema. In contrast to previous models which display a second fluid–fluid transition, the phase behavior of the present model fluid does not result from an *a priori* imposed dependence of the bonding interaction upon bulk density. The zeroth-order solution shows only one, vapor–liquid, phase transition; and a single, continuous locus of density maxima. The results suggest that low-temperature polyamorphic phase transitions in a pure substance can arise from orientation-dependent interactions; and in particular that a phase transition between two dense fluids can be driven by the greater orientational entropy of high density states which are not fully bonded. The predicted phase behavior is, however, sensitive to the level of approximation used to solve the partition function. [S0021-9606(96)52226-9]

I. INTRODUCTION

Network-forming fluids are ubiquitous in nature, water and silica being the most common examples. They are distinguished from ''normal'' molecular fluids by the presence of strong, highly directional, intermolecular attractions that result in the formation of ''bonds'' between molecules that are correctly spaced and oriented with respect to one another. The favorable bonding energy results in the formation of locally structured regions which, due to geometric constraints on the bonded molecules, have lower density than unbonded regions. Such structures in the liquid are local and transient; a fully bonded network exists only in the limit of low temperatures. For example, transient, ''icelike'' regions exist in liquid water, and increase in lifetime and average size as temperature is lowered.[1,2] The geometric requirements for bonding dictate the spatial distribution of bonds and the resulting correlations in molecular positions.[3,4] We refer collectively to this arrangement of bonds and molecular positions as the topology of the network. In fluids such as silica, short- and intermediate-range order in the tetrahedrally coordinated network is resistant to thermal degradation. Consequently the configurational entropy depends weakly on temperature close to the glass transition. This is the ''strong'' extreme of Angell's useful classification scheme for liquids,[5] the ''fragile'' limit being typified by *o*-terphenyl. In the latter case there are no directional bonds and no network. As a result, the configurational entropy close to the glass transition is sensitive to changes in temperature.

Many intriguing properties of liquid silica and water occur at low temperatures (i.e., well below the equilibrium freezing point) and are related to the presence of network structures in the supercooled state. Examples include negative thermal expansion coefficients (α_p) for both silica and water, and increases in isothermal compressibility (κ_T) and isobaric heat capacity (c_p) for water upon supercooling.[4,6]

Interesting properties of network fluids also occur in their amorphous solid states. Both silica[7] and water[8] are known to exhibit polyamorphism.[9] This term refers to distinct amorphous phases that differ in density and local structure. This phenomenon is especially intriguing in water, as an apparently first-order, reversible transition occurs between the two forms of amorphous solid water, LDA and HDA.[8,10,11] Although the amorphous solids are nonergodic on experimental time scales, the presence of distinct, reproducible phases which lack long-range order, and have different densities suggests the existence of an underlying liquid–liquid phase separation for a pure fluid. This is quite remarkable, as liquid–liquid phase transitions are normally associated with phases of different composition.[12]

A full understanding of the effects of the number, spatial orientation, and strength of bonds on the global fluid-phase behavior of network fluids is still lacking. Particular interest lies in the low-temperature behavior and the possibility of polyamorphic transitions. Because the material properties of different amorphous phases may be markedly different (e.g., one amorphous phase of Si is metallic, while another is a semiconductor[13]), polyamorphism is of interest both as a scientific phenomenon and because of its implications for materials processing.

We present here a lattice model of network fluids that shows two fluid–fluid phase transitions when solved with a first-order approximation. This is the first model of its kind to show this behavior based solely upon the molecular interactions described by the model Hamiltonian, without recourse to imposed density dependences on interaction

a)Author to whom correspondence should be addressed.

 0021-9606/96/105(2)/658/15/$10.00

strengths. In contrast, the zeroth-order, or mean-field (MF) solution, shows only a vapor–liquid transition. Both solutions exhibit density anomalies ($\alpha_p<0$).

Our use of the term mean-field requires clarification. In the study of critical phenomena, theories which assume the Helmholtz energy to be analytical at the critical point are called mean-field theories. They all yield the classical critical exponents. In the study of lattice fluids and magnets, the term mean-field denotes the simplest solution technique, in which no account is taken of short-range order. This is also known as the zeroth-order, Bragg-Williams, or molecular field approximation. Throughout the remainder of this paper, we use the term mean-field in the latter sense. The two approximate solution techniques used in this work yield classical critical exponents.

Lattice models have been successfully used to study aspects of the thermodynamics of network fluids. Behavior such as freeze-expansion, density extrema ($\alpha_p=0$), and sharp increases in c_p and κ_T with decreasing temperature have been reproduced by lattice models for water,[14] and by more general models.[15,16] Recent models of Borick *et al.*,[15] Poole *et al.*,[17] and Ponyatovskii *et al.*[18] have shown two fluid–fluid transitions. However, two of these models[15,17] require the additional assumption of an imposed dependence of the bonding interaction on bulk density, while the other[18] is based on the assumption that the molecules exist in one of two ''states'' within the liquid. Our results show that an additional, low temperature phase transition between fluid phases results when a better approximation is used to solve the partition function. In particular, there is no need to impose a density-dependent bonding strength, or to assume particular ''states'' of molecules in the fluid.

Our model is formulated in terms of molecules with waterlike geometry, on a body-centered cubic (BCC) lattice. The molecules interact via nearest-neighbor (nn) attractions and orientation-specific bonds between nn pairs. The open, fully bonded state is a tetrahedral network with a diamond or cubic icelike geometry. In addition to molecular orientations which correspond to the diamond-lattice structure, we also account for molecular orientations of unbonded and partially bonded molecules. Included in these considerations are constraints imposed upon the orientations of partially bonded molecules by molecular geometry. Open structures are stabilized by including a bond-weakening interaction[15] which causes the local energy and density to be negatively correlated, as in liquid water, and also accounts for cooperative effects associated with the formation of local ''icelike'' order.

The paper is organized as follows. The model is formulated in Sec. II. The zeroth- and first-order solutions are discussed in Secs. III and IV, respectively. Finally, in Sec. V we present calculations on the phase behavior, stability limits, and density anomalies predicted by the two solution methods for different interaction strengths and degrees of orientational entropy. We discuss the differences between the predictions of the two solutions, and the molecular origins of the second fluid–fluid phase transition in the first-order solution.

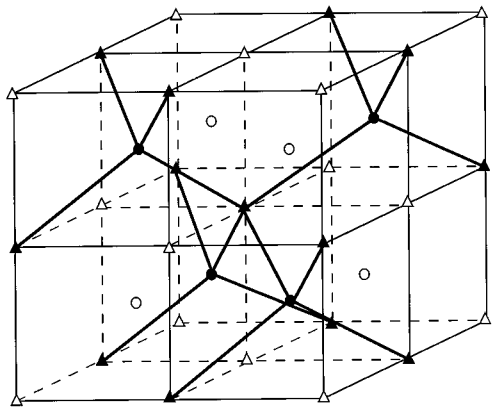

FIG. 1. BCC lattice showing the four sublattices, ●, ▲, ○, and △. Bold lines indicate bonds in the fully bonded, diamondlike structure. In this structure all ● and ▲ are occupied, and all ○ and △ are unoccupied.

II. MODEL FORMULATION

The lattice is composed of body centered cubic unit cells which can be equivalently represented by four, interpenetrating, simple cubic sublattices (denoted with ●, ○, ▲, and △ in Fig. 1). The central site is surrounded by eight nn sites, located at the vertices of the cube as shown in Fig. 2(a). Each occupied nn pair of sites contributes an attractive energy-ϵ. Every molecule has q distinguishable orientations via rotation about the central atom. When a pair of molecules point their bonding arms toward each other, a bond forms and contributes an energy-J. The number and relative orientations of the bonding arms on a molecule is an input to the model. Figure 2(b) illustrates the waterlike geometry used in the present work. The central site represents oxygen, and the molecule has two proton-donor arms (H atoms) and two proton-acceptor arms (electron lone pairs on oxygen); arrows pointing away and toward the central site indicate the donor and acceptor arms, respectively. A bond forms when a donor arm and an acceptor arm point to one another. This restricts the possible orientations of the remaining arms on each of the molecules participating in the bond. The formation of two bonds by the same molecule completely specifies its orientation.

An open network is promoted in this model by imposing an energy penalty for occupied sites which encircle the line of centers of an existing bond. This is illustrated in Fig. 2(b), where the three k sites which lie adjacent to the bond formed between the ij pair weaken that bond by an energy $cJ/3$ ($c>0$) for each occupied k site. All of these sites lie on the same sublattice, which is different from both sublattices occupied by molecules involved in the bond (compare with Fig. 1). The fourth k site in this cell is opposite to the bond, and does not weaken it. Thus, a bond surrounded by occupied sites is ''fully weakened'' and contributes an energy of $-(1-c)J$, as indicated in Fig. 2(a).

The potential energy of the system is expressed mathematically by the following Hamiltonian:

$$\mathscr{H}=-\epsilon\sum_{\langle ij\rangle} n_i n_j - J\sum_{\langle ij\rangle}^{*} n_i n_j \delta_{\sigma_i\sigma_j}\sum_{k(ij)}^{\chi}\frac{1}{\chi}(1-cn_k). \quad (1)$$

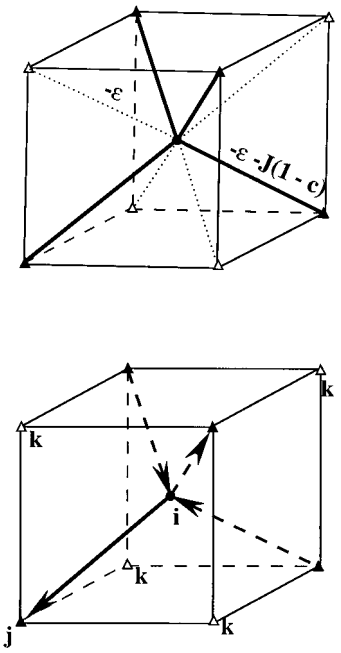

FIG. 2. (a) Illustration of the relative positions of interacting tetrahedral molecules and the associated energies; dotted lines indicate nonbonding pairs, bold full lines indicate bonded pairs. All sites are assumed occupied and with molecules in the correct orientations for bonding if applicable. Bonds are weakened by occupied sites surrounding the line of centers of the bonding pair. See text for notation of interaction energies. (b) Effects of molecular orientations for bond formation; the illustration is for a partially bonded tetrahedral molecule with two proton-donor arms (arrows point away from central molecule) and two proton-acceptor arms (arrows point toward central molecule). The bond is indicated by the filled arrow from the i to the j site. Note the possible bond-weakening sites (three of four k sites), and possible choices for further bonding (indicated by the dashed arrows).

In Eq. (1), n_i is an occupation variable for site i; n_i is 1 if the site is occupied, 0 otherwise. Each molecule is considered to have q distinguishable orientations. The different orientations of the molecule on site i are denoted by a Potts variable $\sigma_i(\sigma_i=1,2,\ldots,q)$. The symbol $\delta_{\sigma_i\sigma_j}$ is given the value 1 if the orientations of molecules i and j are correct for bonding, 0 otherwise. The notation $\langle ij\rangle$ specifies that the summation is over nearest-neighbor pairs. The superscript * on the second summation indicates that restrictions imposed by valency and bond geometry are to be included when determining which nn pairs are allowed to be simultaneously bonded. The third summation is over the bond weakening (k) sites of a given bonding pair (ij). The number of potential bond weakeners (χ) depends upon the molecular geometry. As noted above, χ is 3 for the present treatment.

Ordered, solid phases, which are not included in this work, arise via preferential occupation of one or more sublattices. It is useful, however, to consider the relative stabilities of open- and close-packed ordered phases so as to choose values of the model parameters that will promote open, bonded structures in the fluid over a range of positive pressures. An open, ordered phase similar to that of cubic ice occurs if two sublattices are filled and fully bonded, while the remaining two sublattices are vacant, as shown in Fig. 1. We consider its low-temperature stability relative to the close-packed, ordered structure formed when the four sublattices are filled and fully bonded to each other (e.g., ● with ▲, and ○ with △). This is the analogue of ice VII in our model.

For the solid with an open, diamondlike structure, the number of molecules, M, and sites, N, are related by $M=N/2$, and all molecules lie on the appropriate sublattices and are properly oriented for bonding (see Fig. 1). Therefore no bonds are weakened, and Eq. (1) becomes

$$E_{\text{open}}=-(2M\epsilon+2MJ)=-N(\epsilon+J), \tag{2}$$

from which we can write the enthalpy

$$H_{\text{open}}=2M(Pv_0-\epsilon-J), \tag{3}$$

where v_0 is the volume per site. A similar procedure for the close-packed, fully occupied $(M=N)$ and bonded lattice gives

$$H_{\text{closed}}=M(Pv_0-4\epsilon-2J+2cJ). \tag{4}$$

At 0 K, the Gibbs free energy is equal to the enthalpy, so the equilibrium pressure for the transition between these two structures is found by equating specific enthalpies, from which we find

$$Pv_0=2(cJ-\epsilon). \tag{5}$$

Thus, if $c>\epsilon/J$ there exists a range of positive pressures for which the ground state is open and fully bonded. All values of model parameters used in this work satisfy this condition.

III. MEAN-FIELD SOLUTION

We begin with the grand canonical partition function,

$$\Xi(\mu,V,T)=\sum_{\{n_i\}}\sum_{\{\sigma_i\}} e^{\beta\mu\Sigma_j n_j} e^{-\beta\mathscr{H}}, \tag{6}$$

where $\{n_i\}$ and $\{\sigma_i\}$ indicate summations over all possible distributions of occupation numbers and molecular orientations, respectively. In Eq. (6), μ is the chemical potential, V is the total volume, and T is the temperature. Using Eq. (1),

$$\Xi(\mu,V,T)=\sum_{\{n_i\}}\sum_{\{\sigma_i\}} e^{\beta\mu\Sigma_j n_j} Q_{nb} Q_b, \tag{7}$$

where

$$Q_{nb}=e^{\beta\epsilon\Sigma_{\langle ij\rangle} n_i n_j} \tag{8}$$

and

$$Q_b=e^{\beta(J/3)\Sigma^{*}_{\langle ij\rangle} n_i n_j \delta_{ij} \Sigma^{3}_{k(ij)}(1-cn_k)}. \tag{9}$$

In writing the above expressions we have used $\beta=1/kT$, k is Boltzmann's constant, $\delta_{ij}\equiv\delta_{\sigma_i\sigma_j}$, and have let subscripts nb and b denote nonbonding and bonding contributions to the partition function.

We then average over the distribution of orientation variables, using a single-graph approximation and sphericallization technique.[16,19] This reduces the partition function to summations over occupation variables, and replaces J with a

temperature dependent, effective bonding interaction parameter δJ. Using the techniques detailed in Appendix B, Eq. (7) can then be written

$$\Xi(\mu,V,T)\approx\sum_{\{n_i\}} e^{(\beta\mu+\ln q)\Sigma_j n_j} \times e^{\beta\epsilon\Sigma_{\langle ij\rangle}n_i n_j} e^{\beta\delta J\Sigma^*_{\langle ij\rangle}n_i n_j\Sigma_{k(ij)}(1-c^* n_k)}. \tag{10}$$

In Eq. (10), c^* is formally an effective bond-weakening parameter; expressions for c^* and δJ are given in Appendix B. These quantities require knowledge of p_b, the probability of a bond being formed between a *nn* pair when orientations of the molecules are distributed randomly. We derive an expression for p_b as follows.

Consider a pair of molecules situated on *nn* sites, each with q distinguishable orientations. For a tetrahedral molecule with two donor (D) arms and two acceptor (A) arms, a bond is formed when a $D(A)$ arm is in line with a *nn* $A(D)$ arm. The MF estimate for the bonding probability follows from the assumption that bond formation between a given *nn* pair is independent of bonds formed by that pair with other molecules. However, it should be realized that we still enforce the restriction on the number of bonds possible for a single molecule when evaluating the summation $\Sigma^*_{\langle ij\rangle}$ in Eq. (10) explicitly. Thus each molecule can participate in a maximum of only four bonds simultaneously. In the mean-field approximation each bond is treated independently. With this approximation, p_b is the product of the individual probabilities of each molecule in the pair pointing an arm to one of its *nn* sites, multiplied by a factor to account for the distinguishability of *D*-*A* and *A*-*D* pairings. The probability for one molecule to be pointing an arm to a given *nn* site is equal to the fraction of its q orientations in which one arm is fixed in a given direction. We will denote by n the number of orientations available to a molecule having the direction of one arm fixed. The single molecule probability then is n/q.

To derive a relationship for n in terms of q we note that a molecule with one arm fixed can rotate the other arm(s) through 360°, about the fixed arm. Thus n is essentially the number of increments into which we discretize those 360°. Now consider the central atom to be at the origin of a sphere. We can point a given arm in $n^2/2$ directions (i.e., rotating over 360° in one plane, and over 180° perpendicular to the plane at each point along that circle). We must also include the n orientations due to rotating the other three arms about the axis of the given arm, for each of the $n^2/2$ directions. This gives a total of $n^3/2$ orientations. However, for a molecule with two D and two A arms, this will overcount the number of distinguishable orientations by 2. Applying this to a molecule with a waterlike geometry, we have

$$n^3=4q \tag{11}$$

and

$$p_b=2\left(\frac{n}{q}\right)^2=2\left(\frac{2}{q}\right)^{4/3}, \tag{12}$$

where we must include a factor of 2 in p_b since we can distinguish between bonding as an $A-D$ pair and bonding as a $D-A$ pair, for a selected molecule.

We next apply the mean-field approximation to the occupation variables.[15,16] We denote the fractional occupation of each sublattice by ρ_i $(i=1,\ldots,4)$, and the overall fraction of occupied sites by $\rho(=M/N)$. The equation of state then follows from $PNv_0=kT\ln\Xi$ (using the maximum term of Ξ and the fact that $\rho_1=\rho_2=\rho_3=\rho_4=\rho$ for fluid phases) as

$$P^*=(\mu^*+T^*\ln q)\rho+4x\rho^2-T^*(\rho\ln\rho+(1-\rho)\times\ln(1-\rho))+12\delta J^*\rho^2(1-c^*\rho). \tag{13}$$

The following reduced variables are used in the above expression: $P^*\equiv Pv_0/J$, $\mu^*\equiv\mu/J$, $x\equiv\epsilon/J$, $T^*\equiv kT/J$, and $\delta J^*\equiv\delta J/J$. We can eliminate μ^* from Eq. (13) by realizing that at equilibrium $\ln\Xi(\mu,V,T)$ must satisfy $(\partial\ln\Xi/\partial\rho)_{\mu,V,T}=0$ and thus

$$\left(\frac{\partial P^*}{\partial\rho}\right)=0=\mu^*+T^*\ln q+8x\rho-T^*\ln\left(\frac{\rho}{1-\rho}\right)+12\delta J^*(2\rho-3c^*\rho^2). \tag{14}$$

Rearranging for $(\mu^*+T^*\ln q)$ gives

$$(\mu^*+T^*\ln q)=-8x\rho+T^*\ln\frac{\rho}{1-\rho}-12\delta J^*(2\rho-3c^*\rho^2). \tag{15}$$

Substituting this in Eq. (13) yields

$$P^*=-a^*\rho^2-T^*\ln(1-\rho), \tag{16}$$

with

$$a^*=4x+12\delta J^*(1-2c^*\rho). \tag{17}$$

We see that the MF fluid equation of state has a form similar to that seen in previous, related work on network-fluid, lattice models:[15] a modified van der Waals equation, with a density- and temperature-dependent attractive parameter a^*, and a logarithmic repulsive term in the place of the van der Waals excluded volume term, $kT/(v-b)$. As we show in Appendix A, this equation of state is incapable of showing a second fluid–fluid phase transition. The mean-field solution has essentially blurred all molecular details of bonding via the averaging of the orientational and bonding states. The loss of the details of molecular geometry and connectivity arises because the mean-field expression for p_b assumes orientations of different molecules to be independent, thereby neglecting the cooperative nature of bonding.

IV. EXTENDED QUASICHEMICAL SOLUTION

We begin the first-order or extended quasichemical (QC) solution with the canonical partition function

$$Q(M,V,T)=\sum_E \Omega(M,V,E)e^{-\beta E}, \tag{18}$$

where E is the potential energy corresponding to a configuration with a given M and V, and Ω is the number of distin-

guishable ways of arranging M molecules on $N(=V/v_0)$ lattice sites for a given value of E. Other notation is the same as that introduced previously. In writing Eq. (18) we have omitted contributions to the partition function from kinetic energy terms and from internal degrees of freedom of the molecules; which removes a temperature-dependent, multiplicative term. This does not affect our results, because the equation of state is derived from the derivative of $\ln Q$ with respect to volume at constant temperature (as shown below), and because this multiplicative term contributes equally to the chemical potentials of different phases at equilibrium.

The equation of state $P(\rho,T)$ is obtained from the Helmholtz free energy $A(=-kT\ln Q)$

$$P=-\left(\frac{\partial A}{\partial V}\right)_T=kT\left(\frac{\partial \ln Q}{\partial V}\right)_T, \tag{19}$$

where $A=aN$. We approximate Q by its maximum term, reducing the problem to that of maximizing $\ln Q$, subject to the constraints of ρ and T (or M,N,T).

The method used here is formally identical to that described in Debenedetti *et al.*[20] The lattice is divided into a number of identical, fundamental ''cells.'' The possible configurations within one cell are fully enumerated with the assumption that each cell is independent of all others. The configurations of the full lattice are then approximated by assuming that cells are distributed randomly, with a distribution of cell-configuration probabilities that minimizes the Helmholtz free energy. The geometry of the BCC lattice does not lend itself to a tesselation procedure such as that used in Debenedetti *et al.*;[20] such a procedure would here lead to differentiating between molecules on different sublattices, which is inadequate for the treatment of disordered phases. The number of cells, N_{cells}, is chosen so as to preserve the number of nn site contacts existing in the actual lattice. Thus, $N_{\text{cells}}=N/2$. The fundamental cell is chosen to be large enough to represent all bonded and nonbonded configurations of the central molecule with its nearest neighbors. Thus, the geometry of the model (e.g., bond orientation) is preserved exactly for clusters up to nine molecules. As will be discussed later, this approach does not account for interactions of molecules on the corner sites with molecules in neighboring cells. The choice of $N_{\text{cells}}=N/2$ does, however, preserve the number of nonbonding interactions; but bonds are determined only within the fundamental cell. Therefore the lattice geometry, though used explicitly when enumerating the possible configurations of the fundamental cell, is not preserved when calculating the number of configurations for the entire system, because cells are assumed to be randomly mixed. This does not pose severe problems for disordered phases such as we consider here, but could affect the accuracy of calculations involving phases with long-range order.

We denote the total number of cell configurations by m ($m=98$ in the present model), and denote the number of occupied sites, the energy, and the degeneracy for the jth cell-configuration as n_j, ϵ_j, and ω_j, respectively. By degeneracy of a cell configuration we mean the number of equivalent ways of placing and orienting the given number of molecules while preserving the energy, bonds, relative positions and relative orientations that define that cell configuration. Expressions for ϵ_j and ω_j, can be written *a priori* in terms of the parameters of the model, and are given in Table I, where the possible cell configurations are enumerated (n has the same meaning in Table I as it does in our mean-field solution). The assumption in writing the ω_j expressions in Table I is that each cell is independent of all others with respect to the orientations that molecules on the vertices of the cube may possess. The probability of a given cell configuration from among the entries in Table I is $\omega_j\psi_j$, and thus ψ_j is the probability of observing a cell for which the exact number, placement, and orientations of molecules in the cell correspond to one of the degenerate arrangements of cell configuration j. The values of each ψ_j in the limit of infinite temperature are also given in Table I.

The entries in Table I are to be interpreted in the following manner. Consider entry 37; this describes the cell configuration shown in Fig. 3. From Table I, we see that there are five occupied sites ($A-E$ in Fig. 3), four of which are corner sites ($B-E$). One bond exists (between molecules A and B). There are two molecules ($n_4+n_5+n_6+n_7=2$) which cannot bond to A because of geometric restrictions imposed on the orientations of A by the $A-B$ bond. One molecule (C) weakens the $A-B$ bond ($n_5=1$). The molecule D is opposite the bond and so does not weaken it ($n_4=1$). There are no molecules which simultaneously weaken 2 or 3 bonds ($n_6=n_7=0$). We have now accounted for four of the five molecules using the entries for n_1 to n_7. Therefore the remaining molecule (E) occupies a site which is not excluded from bonding with A, but is not bonded to A because the orientations of the AE pair are not correct for bonding. Note that the configurations in Table I do not have different entries for differences in donor–acceptor and acceptor–donor bonds with the central molecule. These differences are incorporated into the expressions for ω_j.

The number of possible configurations of the system, including molecular orientations and vacancies, is estimated by assuming that the N_{cells} cells are independent of each other and that their m possible realizations are randomly distributed on the lattice, with a frequency of occurrence to be determined as explained below. Since the cells are independent, we write

$$\Omega=\Omega_0\,\frac{N_{\text{cells}}!}{\Pi_{j=1}^{m}((\psi_j N_{\text{cells}})!)^{\omega_j}}. \tag{20}$$

In Eq. (20), Ω_0 is a normalization constant. We determine its value by forcing Ω to be accurate in the high temperature limit, where the distribution of molecules and orientations is random, and thus

$$\Omega_0\,\frac{N_{\text{cells}}!}{\Pi_{j=1}^{m}([\psi_j^{\infty}N_{\text{cells}}]!)^{\omega_j}}=\frac{N!q^{\rho N}}{[\rho N]![(1-\rho)N]!} \tag{21}$$

in which we have denoted the infinite temperature value of ψ_j by ψ_j^{∞}. To determine the energy we use

TABLE I. Configurations, energies, and degeneracies of a fundamental cell.[a]

j	$\mathbf{n}_1$	$\mathbf{n}_2$	$\mathbf{n}_3$	$\mathbf{n}_4$	$\mathbf{n}_5$	$\mathbf{n}_6$	$\mathbf{n}_7$	ω_j	ϵ_j/J	ψ_j^{∞}
1	0	0	0	0	0	0	0	1	0	$(1-\rho)^9$
2	1	0	0	0	0	0	0	q	0	$\rho(1-\rho)^8/q$
3	1	1	0	0	0	0	0	$8q$	0	$\rho(1-\rho)^8/q$
4	2	1	1	0	0	0	0	$16n^2$	$-x-1$	$\rho^2(1-\rho)^7/q^2$
5	2	1	0	0	0	0	0	$8q^2-\omega_4$	$-x$	$\rho^2(1-\rho)^7/q^2$
6	2	2	0	0	0	0	0	$28q^2$	0	$\rho^2(1-\rho)^7/q^2$
7	3	2	2	0	0	0	0	$120n^2$	$-2x-2$	$\rho^3(1-\rho)^6/q^3$
8	3	2	1	0	0	0	0	$48n^2(q-3)$	$-2x-1$	$\rho^3(1-\rho)^6/q^3$
9	3	2	1	1	0	0	0	$16n^2q$	$-2x-1$	$\rho^3(1-\rho)^6/q^3$
10	3	2	1	0	1	0	0	$48n^2q$	$-2x-1+c/3$	$\rho^3(1-\rho)^6/q^3$
11	3	2	0	0	0	0	0	$28q^3-\Sigma\omega_j$, $j=7...10$	$-2x$	$\rho^3(1-\rho)^6/q^3$
12	3	3	0	0	0	0	0	$56q^3$	0	$\rho^3(1-\rho)^6/q^3$
13	4	3	3	0	0	0	0	$48n^3$	$-3x-3$	$\rho^4(1-\rho)^5/q^4$
14	4	3	2	0	0	0	0	$240n^2(q-n)$	$-3x-2$	$\rho^4(1-\rho)^5/q^4$
15	4	3	2	0	1	0	0	$240n^2q$	$-3x-2+c/3$	$\rho^4(1-\rho)^5/q^4$
16	4	3	2	0	0	1	0	$240n^2q$	$-3x-2+2c/3$	$\rho^4(1-\rho)^5/q^4$
17	4	3	1	0	0	0	0	$48n^2(q^2-6q+3n)$	$-3x-1$	$\rho^4(1-\rho)^5/q^4$
18	4	3	1	1	0	0	0	$48n^2q(q-3)$	$-3x-1$	$\rho^4(1-\rho)^5/q^4$
19	4	3	1	0	1	0	0	$144n^2q(q-3)$	$-3x-1+c/3$	$\rho^4(1-\rho)^5/q^4$
20	4	3	1	1	1	0	0	$48n^2q^2$	$-3x-1+c/3$	$\rho^4(1-\rho)^5/q^4$
21	4	3	1	0	2	0	0	$48n^2q^2$	$-3x-1+2c/3$	$\rho^4(1-\rho)^5/q^4$
22	4	3	0	0	0	0	0	$56q^4-\Sigma\omega_j$, $j=13...21$	$-3x$	$\rho^4(1-\rho)^5/q^4$
23	4	4	0	0	0	0	0	$70q^4$	0	$\rho^4(1-\rho)^5/q^4$
24	5	4	4	0	0	0	0	$12n^4$	$-4x-4$	$\rho^5(1-\rho)^4/q^5$
25	5	4	3	0	0	0	0	$48n^3(q-n)$	$-4x-3$	$\rho^5(1-\rho)^4/q^5$
26	5	4	3	0	0	1	0	$144n^3q$	$-4x-3+2c/3$	$\rho^5(1-\rho)^4/q^5$
27	5	4	3	0	0	0	1	$48n^3q$	$-4x-3+c$	$\rho^5(1-\rho)^4/q^5$
28	5	4	2	0	0	0	0	$120n^2(q-n)^2$	$-4x-2$	$\rho^5(1-\rho)^4/q^5$
29	5	4	2	0	1	0	0	$480n^2q(q-n)$	$-4x-2+c/3$	$\rho^5(1-\rho)^4/q^5$
30	5	4	2	0	0	1	0	$480n^2q(q-n)$	$-4x-2+2c/3$	$\rho^5(1-\rho)^4/q^5$
31	5	4	2	0	2	0	0	$120n^2q^2$	$-4x-2+2c/3$	$\rho^5(1-\rho)^4/q^5$
32	5	4	2	0	1	1	0	$480n^2q^2$	$-4x-2+c/3$	$\rho^5(1-\rho)^4/q^5$
33	5	4	2	0	0	2	0	$120n^2q^2$	$-4x-2+4c/3$	$\rho^5(1-\rho)^4/q^5$
34	5	4	1	0	0	0	0	$16n^2(q^3-9q^2+9nq-3n^2)$	$-4x-1$	$\rho^5(1-\rho)^4/q^5$
35	5	4	1	1	0	0	0	$48n^2q(q^2-6q+3n)$	$-4x-1$	$\rho^5(1-\rho)^4/q^5$
36	5	4	1	0	1	0	0	$144n^2q(q^2-6q+3n)$	$-4x-1+c/3$	$\rho^5(1-\rho)^4/q^5$
37	5	4	1	1	1	0	0	$144n^2q^2(q-n)$	$-4x-1+c/3$	$\rho^5(1-\rho)^4/q^5$
38	5	4	1	0	2	0	0	$144n^2q^2(q-n)$	$-4x-1+2c/3$	$\rho^5(1-\rho)^4/q^5$
39	5	4	1	1	2	0	0	$48n^2q^3$	$-4x-1+2c/3$	$\rho^5(1-\rho)^4/q^5$
40	5	4	1	0	3	0	0	$16n^2q^3$	$-4x-1+c$	$\rho^5(1-\rho)^4/q^5$
41	5	4	0	0	0	0	0	$70q^5-\Sigma\omega_j$, $j=24...40$	$-4x$	$\rho^5(1-\rho)^4/q^5$
42	5	5	0	0	0	0	0	$56q^5$	0	$\rho^5(1-\rho)^4/q^5$
43	6	5	4	0	0	0	1	$48n^4q$	$-5x-4+c$	$\rho^6(1-\rho)^3/q^6$
44	6	5	3	0	0	1	0	$144n^3q(q-n)$	$-5x-3+2c/3$	$\rho^6(1-\rho)^3/q^6$
45	6	5	3	0	0	0	1	$48n^3q(q-n)$	$-5x-3+c/3$	$\rho^6(1-\rho)^3/q^6$
46	6	5	3	0	0	2	0	$144n^3q^2$	$-5x-3+4c/3$	$\rho^6(1-\rho)^3/q^6$
47	6	5	3	0	0	1	1	$144n^3q^2$	$-5x-3+5c/3$	$\rho^6(1-\rho)^3/q^6$
48	6	5	2	0	1	0	0	$240n^2q(q-n)^2$	$-5x-2+c/3$	$\rho^6(1-\rho)^3/q^6$
49	6	5	2	0	0	1	0	$240n^2q(q-n)^2$	$-5x-2+2c/3$	$\rho^6(1-\rho)^3/q^6$
50	6	5	2	0	2	0	0	$240n^2q^2(q-n)$	$-5x-2+2c/3$	$\rho^6(1-\rho)^3/q^6$
51	6	5	2	0	1	1	0	$960n^2q^2(q-n)$	$-5x-2+c$	$\rho^6(1-\rho)^3/q^6$
52	6	5	2	0	0	2	0	$240n^2q^2(q-n)$	$-5x-2+4c/3$	$\rho^6(1-\rho)^3/q^6$
53	6	5	2	0	2	1	0	$240n^2q^3$	$-5x-2+4c/3$	$\rho^6(1-\rho)^3/q^6$
54	6	5	2	0	1	2	0	$240n^2q^3$	$-5x-2+5c/3$	$\rho^6(1-\rho)^3/q^6$
55	6	5	1	1	0	0	0	$16n^2q(q^3-9q^2+9nq-3n^2)$	$-5x-1$	$\rho^6(1-\rho)^3/q^6$
56	6	5	1	0	1	0	0	$48n^2q(q^3-9q^2+9nq-3n^2)$	$-5x-1+c/3$	$\rho^6(1-\rho)^3/q^6$
57	6	5	1	1	1	0	0	$144n^2q^2(q^2-6q+3n)$	$-5x-1+c/3$	$\rho^6(1-\rho)^3/q^6$
58	6	5	1	0	2	0	0	$144n^2q^2(q^2-6q+3n)$	$-5x-1+2c/3$	$\rho^6(1-\rho)^3/q^6$
59	6	5	1	1	2	0	0	$144n^2q^3(q-3)$	$-5x-1+2c/3$	$\rho^6(1-\rho)^3/q^6$
60	6	5	1	0	3	0	0	$48n^2q^3(q-3)$	$-5x-1+c$	$\rho^6(1-\rho)^3/q^6$
61	6	5	1	1	3	0	0	$16n^2q^4$	$-5x-1+c$	$\rho^6(1-\rho)^3/q^6$
62	6	5	0	0	0	0	0	$56q^6-\Sigma\omega_j$, $j=43...61$	$-5x$	$\rho^6(1-\rho)^3/q^6$
63	6	6	0	0	0	0	0	$28q^6$	0	$\rho^6(1-\rho)^3/q^6$
64	7	6	4	0	0	0	2	$72n^4q^2$	$-6x-4+2c$	$\rho^7(1-\rho)^2/q^7$
65	7	6	3	0	0	2	0	$144n^3q^2(q-n)$	$-6x-3+4c/3$	$\rho^7(1-\rho)^2/q^7$
66	7	6	3	0	0	1	3	$144n^3q^2(q-n)$	$-6x-3+5c/3$	$\rho^7(1-\rho)^2/q^7$

TABLE I. (*Continued.*)

j	$\mathbf{n}_1$	$\mathbf{n}_2$	$\mathbf{n}_3$	$\mathbf{n}_4$	$\mathbf{n}_5$	$\mathbf{n}_6$	$\mathbf{n}_7$	ω_j	ϵ_j/J	ψ_j^∞
67	7	6	3	0	0	3	0	$48n^3q^3$	$-6x-3+2c$	$\rho^7(1-\rho)^2/q^7$
68	7	6	3	0	0	2	1	$144n^3q^3$	$-6x-3+7c/3$	$\rho^7(1-\rho)^2/q^7$
69	7	6	2	0	2	0	0	$120n^2q^2(q-n)^2$	$-6x-2+2c/3$	$\rho^7(1-\rho)^2/q^7$
70	7	6	2	0	1	1	0	$480n^2q^2(q-n)^2$	$-6x-2+c$	$\rho^7(1-\rho)^2/q^7$
71	7	6	2	0	0	2	0	$120n^2q^2(q-n)^2$	$-6x-2+4c/3$	$\rho^7(1-\rho)^2/q^7$
72	7	6	2	0	2	1	0	$480n^2q^3(q-n)$	$-6x-2+4c/3$	$\rho^7(1-\rho)^2/q^7$
73	7	6	2	0	1	2	0	$480n^2q^3(q-n)$	$-6x-2+5c/3$	$\rho^7(1-\rho)^2/q^7$
74	7	6	2	0	2	2	0	$120n^2q^4$	$-6x-2+2c$	$\rho^7(1-\rho)^2/q^7$
75	7	6	1	1	1	0	0	$48n^2q^2(q^3-9q^2+9nq-3n^2)$	$-6x-1+c/3$	$\rho^7(1-\rho)^2/q^7$
76	7	6	1	0	2	0	0	$48n^2q^2(q^3-9q^2+9nq-3n^2)$	$-6x-1+2c/3$	$\rho^7(1-\rho)^2/q^7$
77	7	6	1	1	2	0	0	$144n^2q^3(q^2-6q+3n)$	$-6x-1+2c/3$	$\rho^7(1-\rho)^2/q^7$
78	7	6	1	0	3	0	0	$48n^2q^3(q^2-6q+3n)$	$-6x-1+c$	$\rho^7(1-\rho)^2/q^7$
79	7	6	1	1	3	0	0	$48n^2 2q^4(q-3)$	$-6x-1+c$	$\rho^7(1-\rho)^2/q^7$
80	7	6	0	0	0	0	0	$28q^7-\Sigma\omega_j$, $j=64...79$	$-6x$	$\rho^7(1-\rho)^2/q^7$
81	7	7	0	0	0	0	0	$8q^7$	0	$\rho^7(1-\rho)^2/q^7$
82	8	7	4	0	0	0	3	$48n^4q^3$	$-7x-4+3c$	$\rho^8(1-\rho)/q^8$
83	8	7	3	0	0	3	0	$48n^3q^3(q-n)$	$-7x-3+2c$	$\rho^8(1-\rho)/q^8$
84	8	7	3	0	0	2	1	$144n^3q^3(q-n)$	$-7x-3+7c/3$	$\rho^8(1-\rho)/q^8$
85	8	7	3	0	0	3	1	$48n^3q^4$	$-7x-3+3c$	$\rho^8(1-\rho)/q^8$
86	8	7	2	0	2	1	0	$240n^2q^3(q-n)^2$	$-7x-2+4c/3$	$\rho^8(1-\rho)/q^8$
87	8	7	2	0	1	2	0	$240n^2q^3(q-n)^2$	$-7x-2+5c/3$	$\rho^8(1-\rho)/q^8$
88	8	7	2	0	2	2	0	$240n^2q^4(q-n)$	$-7x-2+2c$	$\rho^8(1-\rho)/q^8$
89	8	7	1	1	2	0	0	$48n^2q^3(q^3-9q^2+9nq-3n^2)$	$-7x-1+2c/3$	$\rho^8(1-\rho)/q^8$
90	8	7	1	0	3	0	0	$16n^2q^3(q^3-9q^2+9nq-3n^2)$	$-7x-1+c$	$\rho^8(1-\rho)/q^8$
91	8	7	1	1	3	0	0	$48n^2q^4(q^2-6q+3n)$	$-7x-1+c$	$\rho^8(1-\rho)/q^8$
92	8	7	0	0	0	0	0	$8q^8-\Sigma\omega_j$, $j=82...91$	$-7x$	$\rho^8(1-\rho)/q^8$
93	8	8	0	0	0	0	0	q^8	0	$\rho^8(1-\rho)/q^8$
94	9	8	4	0	0	0	4	$12n^4q^4$	$-8x-4+4c$	ρ^9/q^9
95	9	8	3	0	0	3	1	$48n^3q^4(q-n)$	$-8x-3+3c$	ρ^9/q^9
96	9	8	2	0	2	2	0	$120n^2q^4(q-n)^2$	$-8x-2+2c$	ρ^9/q^9
97	9	8	1	1	3	0	0	$16n^2q^4(q^3-9q^2+9nq-3n^2)$	$-8x-1+c$	ρ^9/q^9
98	9	8	0	0	0	0	0	$q^9-\Sigma\omega_j$, $j=94...97$	$-8x$	ρ^9/q^9

[a] $\mathbf{n}_1$: number of occupied sites; $\mathbf{n}_2$: number of occupied corner sites; $\mathbf{n}_3$: number of bonds; $\mathbf{n}_4-\mathbf{n}_7$: molecules which cannot bond to the central molecule because of constraints due to existing bonds, and which simultaneously weaken existing bonds: $\mathbf{n}_4$ denotes the number of such molecules weakening 0 bonds; $\mathbf{n}_5$, the number weakening 1 bond; $\mathbf{n}_6$, the number weakening 2 bonds; $\mathbf{n}_7$, the number weakening 3 bonds.

$$E=N_{\text{cells}}\sum_{j=1}^{m}\epsilon_j\omega_j\psi_j\,. \tag{22}$$

Our problem is that of maximizing $\ln\Omega-\beta E$ with respect to the $\{\psi_j\}$ at a given T and ρ. Note, however, that the ψ_j values are not completely independent, as the distribution $\{\psi_j\}$ must satisfy the material balances on occupied sites and vacancies,

$$\rho=\frac{1}{\alpha}\sum_{j=1}^{m}\psi_j\omega_j n_j\,, \tag{23}$$

$$(1-\rho)=\frac{1}{\alpha}\sum_{j=1}^{m}\psi_j\omega_j(\alpha-n_j), \tag{24}$$

with the number of sites per cell denoted by $\alpha(=9)$. The normalization of $\{\psi_j\}$ follows from the overall material balance on sites [which is just a linear combination of Eqs. (23) and (24)]

$$1=\sum_{j=1}^{m}\psi_j\omega_j\,. \tag{25}$$

Mathematically, the material balances remove two degrees of freedom from the problem of minimizing the free energy with respect to $\{\psi_j\}$. We thus have two dependent probabilities, which we call ψ_c and ψ_d. The manner in which these are included in the derivation is shown in detail in Appendix C.

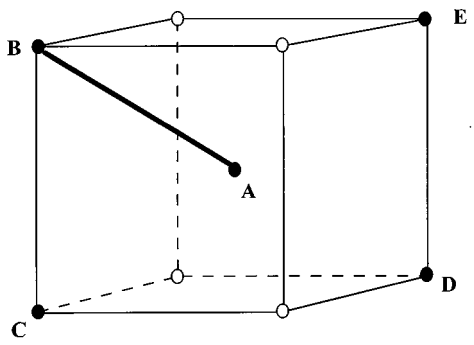

FIG. 3. Configuration 37 from Table I. Sublattices are not distinguished in this diagram. Occupied and unoccupied sites are indicated by filled and unfilled circles, respectively. Identity of bond arms as donor or acceptor, and orientations of unbonded arms are not included. Refer to text for labeling of molecules *A* to *E*.

Returning now to Eq. (21) and solving for $\ln \Omega_o$ [using Stirling's approximation and Eq. (25)] gives

$$\ln \Omega_o = \frac{N}{2} \sum_{j=1}^{m} \omega_j \psi_j^{\infty} \ln \psi_j^{\infty} - N[\rho \ln(\rho/q) + (1-\rho)\ln(1-\rho)]. \tag{26}$$

We now have expressions for all the terms in Eq. (18). Equating the partition function to its maximum term, we write for the Helmholtz free energy per site ($a = A/N$) from Eqs. (18), (20), (22), and (26):

$$a = \frac{1}{2}\left[\sum_{j=1}^{m} \epsilon_j \omega_j \psi_j + kT\left(\sum_{j=1}^{m} \omega_j \psi_j \ln \psi_j - \sum_{j=1}^{m} \omega_j \psi_j^{\infty} \ln \psi_j^{\infty} + 2\rho \ln \frac{\rho}{q} + 2(1-\rho)\ln(1-\rho)\right)\right], \tag{27}$$

where the $\{\psi_j\}$ are to be determined by maximizing the generic term in the partition function. We now write an expression for pressure using a more convenient form of Eq. (19)

$$P v_o = \rho\left(\frac{\partial a}{\partial \rho}\right)_T - a. \tag{28}$$

Using Eq. (28) gives (see also, Appendix C)

$$P v_o = -a + \frac{\rho kT}{2}\left[-\sum_{j=1}^{m} \omega_j \left(\frac{\partial \psi_j^{\infty}}{\partial \rho}\right)(1 + \ln \psi_j^{\infty}) + \frac{9}{n_c - n_d}\left[\beta(\epsilon_c - \epsilon_d) - \ln\left(\frac{\psi_d}{\psi_c}\right)\right] + 2 \ln \frac{\rho}{q(1-\rho)}\right] \tag{29}$$

and with $\mu = (\partial a/\partial \rho)_T$ we have also

$$\mu = \frac{kT}{2}\left[-\sum_{j=1}^{m} \omega_j \left(\frac{\partial \psi_j^{\infty}}{\partial \rho}\right)(1 + \ln \psi_j^{\infty}) + \frac{9}{n_c - n_d}\left[\beta(\epsilon_c - \epsilon_d) - \ln\left(\frac{\psi_d}{\psi_c}\right)\right] + 2 \ln \frac{\rho}{q(1-\rho)}\right]. \tag{30}$$

Provided we have the equilibrium $\{\psi_j\}$ at a given T and ρ, we now have P and μ as a function of T and ρ. In order to determine the $\{\psi_j\}$, we use the equilibrium requirement that A (and thus a) be a minimum with respect to variations in the independent ψ_j's at constant ρ.

$$0 = \left(\frac{\partial a}{\partial \psi_j}\right)_{T,\rho,\{\psi_j\}_{j \neq c,d}} \qquad j = 1,\ldots,m (j \neq c,d). \tag{31}$$

From Eq. (31) we obtain (see Appendix C) the desired distribution of $\{\psi_j\}$ with $j \neq c,d$. It is given by

$$\ln\left(\frac{\psi_j}{\psi_c}\right) = \frac{n_c - n_j}{n_c - n_d} \ln r - \beta\left(\epsilon_j + \epsilon_c \frac{(n_d - n_j)}{(n_c - n_d)} + \epsilon_d \frac{(n_j - n_c)}{(n_c - n_d)}\right), \tag{32}$$

where $r \equiv \psi_d/\psi_c$. Using this set of equations we rearrange Eqs. (23) and (24) to read

$$\rho = \psi_c \theta, \tag{33}$$

$$1 - \rho = \psi_c \gamma, \tag{34}$$

which can be combined to give

$$\rho(r,T) = \frac{\theta}{\theta + \gamma}, \tag{35}$$

with

$$\theta = \frac{1}{9}\left(\sum_{j}^{*} \frac{\psi_j}{\psi_c} \omega_j n_j + \omega_c n_c + \omega_d n_d r\right), \tag{36}$$

$$\gamma = \frac{1}{9}\left(\sum_{j}^{*} \frac{\psi_j}{\psi_c} \omega_j (9 - n_j) + \omega_c (9 - n_c) + \omega_d (9 - n_d) r\right). \tag{37}$$

Here the symbol * denotes a summation over $j \neq c,d$. The structure of the equations is therefore

$$P = P(\rho, r, T), \tag{38}$$

$$\rho = \rho(r,T), \tag{39}$$

$$\mu = \mu(\rho, r, T). \tag{40}$$

This system is solved by fixing ρ and T; solving (numerically) for r in Eq. (35); and using (r,ρ,T) to calculate P and μ.

V. RESULTS AND DISCUSSION

We now present phase diagrams, stability limits, and loci of density extrema for the QC and MF solutions. Calculations were performed for a range of values of the model parameters. The values for the ratio of nonbonding to bonding strengths (x), the bond-weakening penalty as a fraction of bond strength (c), and the number of distinguishable orientations of a molecule (q) were systematically varied over the ranges [0.1,0.53], [0.3,0.8], and [12,240], respectively. The values for x were based on the assumption that bonding interactions are approximately an order of magnitude stronger than nonbonding interactions (e.g., hydrogen bond strengths relative to van der Waals attractions[3]). The values for c were chosen to satisfy $x < c < 1$, as discussed in Sec. II. The lower bound of 12 for q corresponds to the distinguishable orientations of a molecule which is able to point its arms at only its nn sites; the upper bound was chosen as 240 after determining that further increases in q caused only minor changes in the phase diagrams.

We first consider the QC results, using the case shown in Fig. 4 ($x = 0.2$, $q = 24$, $c = 0.8$) as a reference, and the changes that result when c, x, and q are varied. We begin with the phase behavior; density anomalies are considered

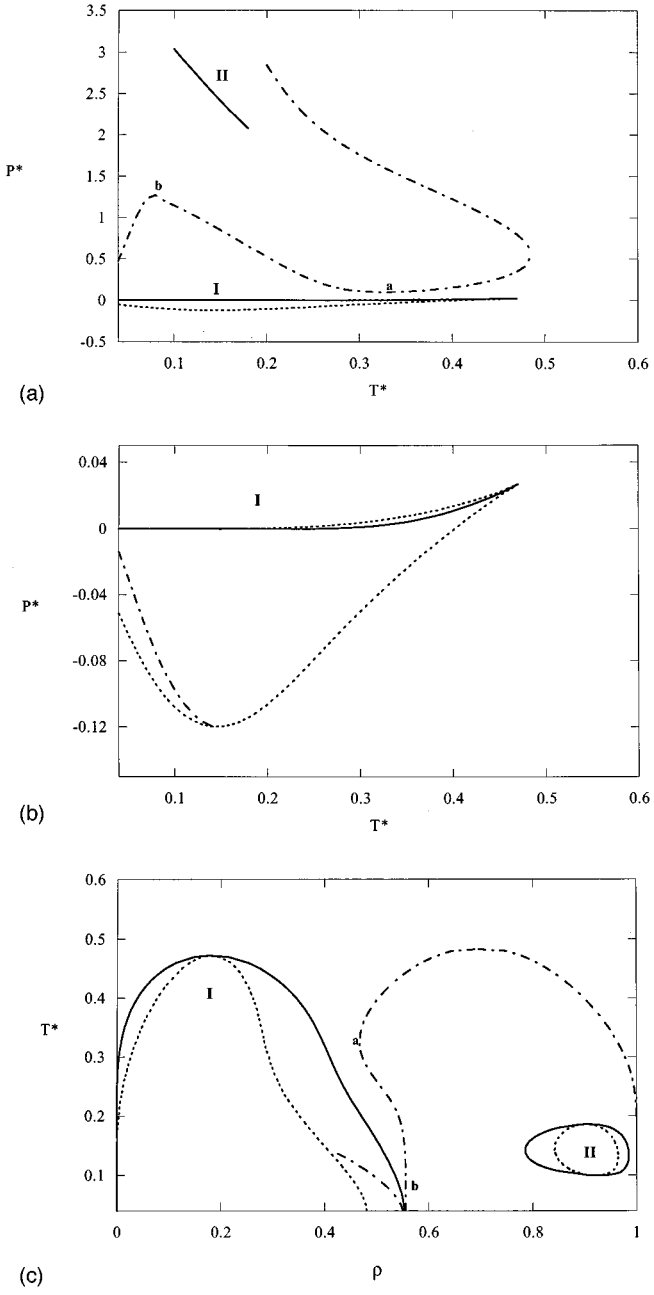

FIG. 4. (a),(b) PT and (c) $T\rho$ projections of the binodals (solid lines), spinodals (dotted lines), and TMD loci (dot–dashed lines) for the case $x=0.2$, $c=0.8$, $q=24$, QC solution. $T^*=kT/J$; $P^*=Pv_0/J$; v_0=volume per site. An enlarged view of the low P^* region of (a) is shown in (b). The TMD from (b), and the spinodals for II are not resolvable on the scale of the plot in (a). Refer to the text for the explanation of a and b.

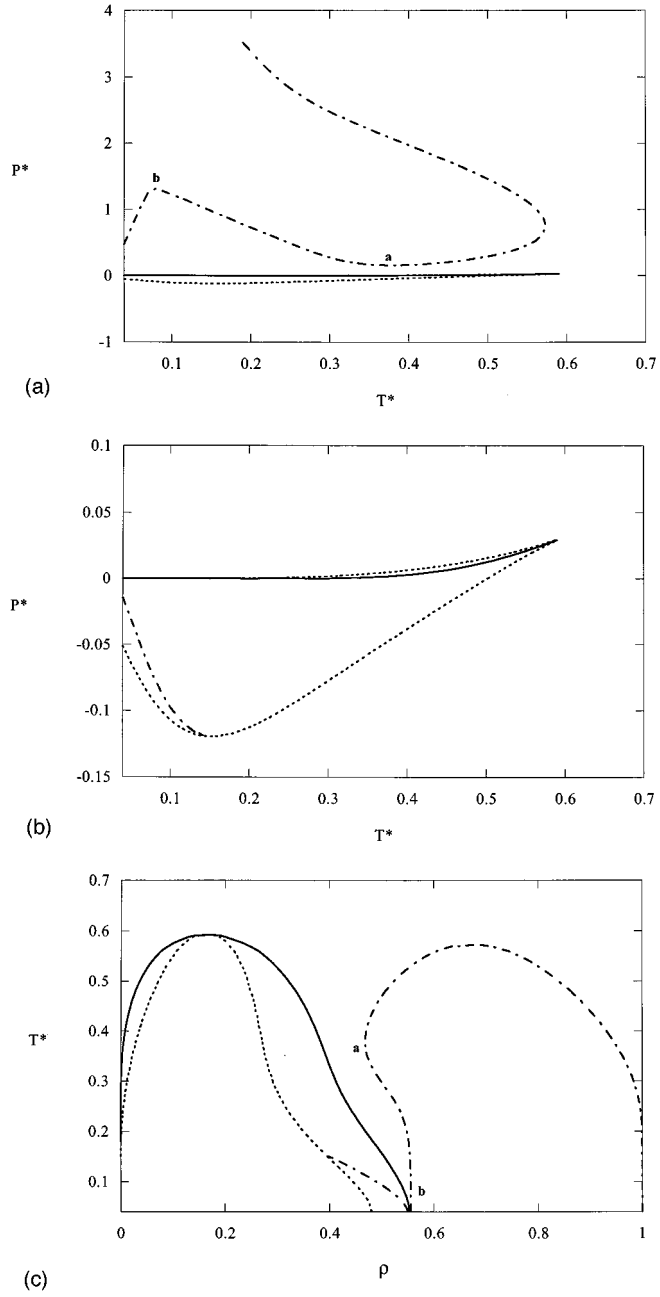

FIG. 5. (a),(b) PT and (c) $T\rho$ diagrams from the QC solution for $x=0.2$, $c=0.8$, $q=12$; notation is as in Fig. 4. See comments in caption to Fig. 4.

below. The salient feature is the existence of two phase transitions (I,II) between disordered phases. For all cases in which the second fluid–fluid transition (II) is observed, it has both upper and lower consolute temperatures (UCT and LCT). We refer to the lowest density phase as the vapor, and to the intermediate and high density phases as liquids, $L1$ and $L2$. The difference between the two liquid densities, and between the UCT and LCT, decreases as either c or x decreases. The second phase transition disappears for low enough values of c or q. Figure 5 illustrates this for the case $q=12$, $c=0.8$, $x=0.2$. The implications of these trends for the existence of the liquid–liquid transition will be discussed below.

The critical temperature (T_c) and pressure (P_c) for transition I (VLE) are always greater than the UCT and the corresponding pressure for II. The density of the coexisting phases is very sensitive to changes in q. This is illustrated in Fig. 6 ($q=240$). Comparison with Fig. 4(c) shows that increasing the orientational entropy causes a density extremum to appear along the $L1$ branch; T_c to decrease slightly; a broadening of the density difference between coexisting $L1$ and $L2$ phases (transition II); and a decrease in the LCT. The

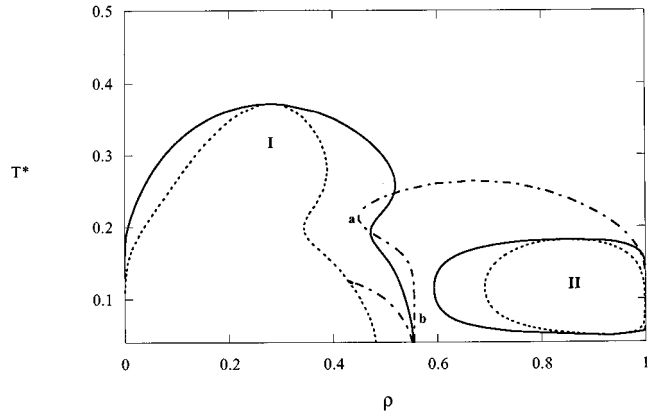

FIG. 6. $T\rho$ diagram from the QC solution for $x=0.2$, $c=0.8$, $q=240$; notation is as in Fig. 4.

relative strength of the nonbonding to the bonding interactions, $x(=\epsilon/J)$, has a pronounced effect on the vapor–liquid transition, but affects transition II only slightly. This is illustrated in Fig. 7 ($q=240$, $x=0.53$). Comparison with Fig. 6 shows that weakening the bonding strength relative to the nonbonding interactions causes the density along the $L1$ branch of I to increase, and raises T_c. In all cases, the density along the $L1$ branch of transition I approaches 5/9 in the limit of zero temperature. This arises from the open ground state (i.e., configuration 24 in Table I), in which five of the nine sites are occupied.

There are pronounced density anomalies for all cases. Starting at high pressure and density [see, e.g., Figs. 4(a) and 4(c)] the locus of density maxima becomes a locus of density minima at point a. At point b the character of the locus reverts to density maxima, and remains so as it approaches the density of the $L1$ branch of transition I in the limit of zero temperature. Thus, in the PT plane the segment ab is a locus of isochore maxima, while the remaining locus represents isochore minima. As can be seen in Fig. 7, the continuity of the locus of density extrema is interrupted at high

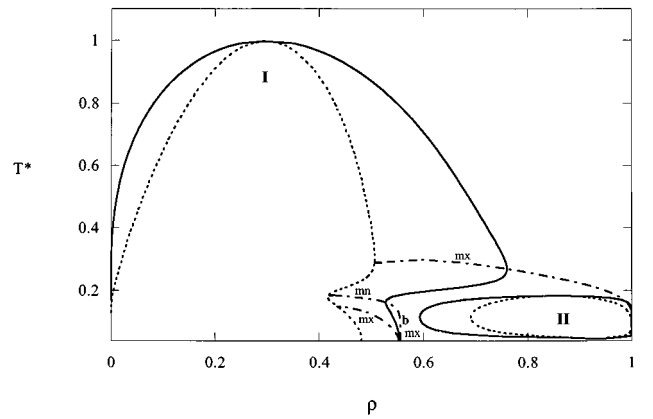

FIG. 7. $T\rho$ diagram from the QC solution for $x=0.53$, $c=0.8$, $q=240$; notation is as in Fig. 4. The TMD locus is unstable (not shown) at the point denoted by a in Fig. 4. mx and mn denote respectively segments of the TMD for which the density extrema are maxima and minima.

enough values of x by intersection with the spinodal branch along which $L1$ becomes unstable with respect to the vapor. A seemingly disconnected locus of density maxima also exists in the region where $L1$ is metastable with respect to the vapor. This locus always exhibits the qualitative behavior shown in Fig. 4(a) and 4(b): It has a negative slope in the PT plane and intersects the $L1$ branch of the spinodal for transition I, causing it to retrace toward higher pressures at low temperatures. The maximum temperature at which density anomalies occur increases as c is increased. These basic features of the TMD are preserved in all cases investigated.

In general, the MF results are significantly different from those discussed above. The most obvious difference is that the $L1-L2$ transition cannot occur (see also Appendix A). In addition, the TMD forms a single locus of density maxima. The MF phase behavior and density anomalies can be categorized according to the behavior of the TMD locus and the liquid spinodal. In all cases studied here, the PT projection of the TMD is negatively sloped over some region of the phase diagram, and has one of the following two forms: (1) The TMD locus is negatively sloped at all pressures, and intercepts the liquid spinodal; the intersection point is necessarily a minimum in the liquid spinodal (i.e., the retracing spinodal scenario consistent with the stability-limit conjecture[21]). (2) The TMD locus retraces toward low temperatures and does not intersect the liquid spinodal (i.e., the retracing-TMD scenario[22]). An example of the retracing TMD scenario is shown in Fig. 8 for $q=24$, $c=0.8$, and $x=0.2$. Upon decreasing c, or increasing q or x, the behavior changes to that of the retracing-spinodal scenario.

As q or x is increased, T_c increases, the $T-\rho$ projections of the binodal and spinodal curves become more symmetric about $\rho=0.5$, and the TMD intersects the liquid spinodal, causing it to retrace. As c increases, the value of the critical density decreases, the maximum temperature for density anomalies increases, and the TMD and liquid spinodal curves show behavior consistent with the retracing TMD scenario.

The TMD and phase behaviors in the MF solution are similar to earlier results for solutions of simpler models with the MF approximation.[15,16] This results from the MF treatment of the bonding probability as an average value for all molecules, regardless of a given molecule's participation in other bonds. The assumption that all bonds form with probability p_b significantly underestimates the chance of bonding for molecules which are already involved in one or more bonds. As an example of this, consider a molecule which is involved in one bond. The chance of it pointing one if its remaining bonding arms toward a nn site is $3/n$, or $3/(4q)^{1/3}$. Assume that a completely nonbonded molecule occupies one of the nn sites with which a second bond could form. The bonding probability is then $3/n$, which is greater than $p_b(=2^{7/3}/q^{4/3})$ for all physically meaningful values of q [i.e., $(3/n)/p_b=3q/8$; $q\geqslant 12$]. This error becomes more significant at higher densities and at lower temperatures, which are the conditions of particular interest for investigating the possibility of polyamorphic transitions.

The errors at high density and low temperature are borne

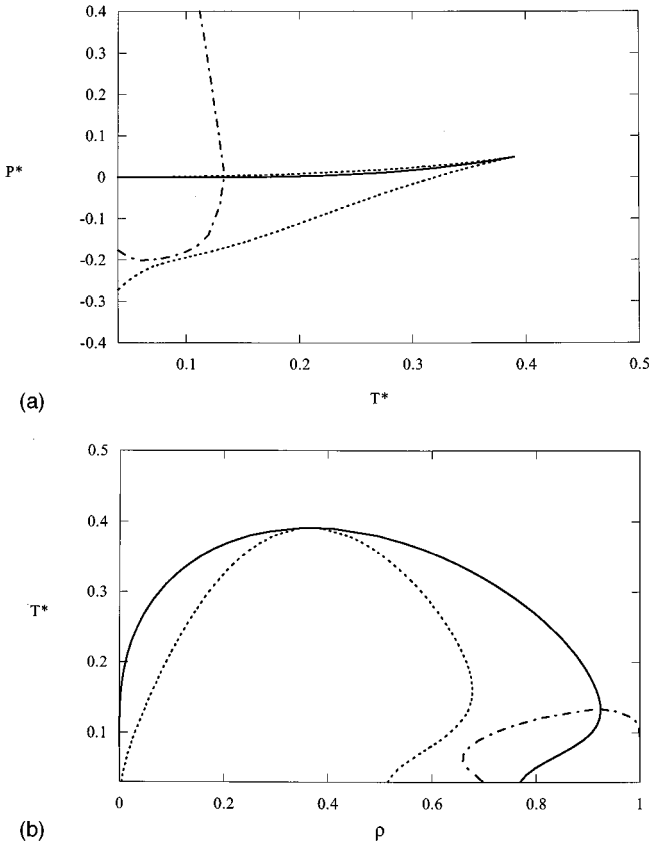

FIG. 8. MF results for $x=0.2$, $c=0.8$, $q=240$, notation is as in Fig. 4.

out in the markedly different behaviors that the QC solution predicts when compared to the MF results. Accurate treatment of just the first shell of bonding neighbors produces solutions with a second fluid–fluid transition. This provides an example of the cooperative nature of bond formation in network fluids, and clearly shows an inherent weakness in the MF solution.

Although the QC treatment is an improvement over the MF solution, it is still not exact. The most serious limitations arise from the assumption that cells are independent. Also, a notable effect of cell size in our work is that a density of 5/9 is imposed as T approaches zero, inducing the pronounced asymmetry in the $T-\rho$ projection of the VLE binodal. The independence of cells causes corner-site molecules in certain configurations to be treated as having q possible orientations, which denies the possibility of bonding for those molecules. Bonds for these molecules must form with molecules in adjacent cells, and thus are neglected in the QC approximation. In Fig. 3, molecules C and D are in this category. When applied to all cells, all molecules are treated equivalently; a molecule that occupies a site such as C in Fig. 3 for one cell, occupies a site such as E for an adjacent cell. The overall effect, however, is that the possibility of all molecules being fully bonded is not realizable in the QC approximation. It is not obvious what the lack of a fully bonded fluid state has on the accuracy of the phase and TMD behavior. The undercounting of possible bonds is expected to overestimate the energy of the fluid at higher pressures and lower temperatures, but this also overestimates the entropy of the fluid. The net effect on the free energy, and thus the ability of the fluid to exhibit a second fluid–fluid phase transition, cannot be reasoned from only the current results. This will be addressed in work which is presently underway to test the current predictions with computer simulations.

We now consider the origin of transition II. At all temperatures and parameter values considered here, the configurational energy and entropy as a function of volume (at constant T) have the qualitative forms shown respectively in Figs. 9(a) and 9(b) ($T^*=0.15$; x, c, and q as in Fig. 4). The minimum in energy and entropy occurs near $v/v_0=\rho^{-1}=9/5$. It corresponds to a maximally bonded configuration (the fully bonded ground state, configuration 24 in Table I, has $v/v_0=9/5$). The specific volumes of the two liquid phases at equilibrium are indicated in the figure, illustrating the significantly higher energy and entropy of the $L2$ phase relative to the $L1$ phase. At temperatures between the LCT and UCT the entropy gain at high densities stabilizes the $L2$ phase; the $L1$ phase is always favored energetically. The essential role that the orientational entropy of the unbonded and partially bonded molecules plays in the stabilization of $L2$ is evident from the sensitivity of transition II to the value of q, as noted earlier when comparing Figs. 4 and 5. Because $L1$ is favored energetically and $L2$ is favored entropically, their opposing contributions to the free energy can balance over only a limited range of temperatures. Accordingly, the first-order transition between two distinct phases possesses both an LCT and an UCT. Below the LCT the entropic contributions are too small to stabilize $L2$; above the UCT, the entropic contributions are too large. In neither case does isothermal compression of $L1$ lead to a new phase.

It was noted earlier that the existence of the second phase transition is dependent upon the magnitude of the bond weakening parameter c. Figure 9(c) ($c=0.3$) shows the effect on the $U(v)$ curve of decreasing c, for the same temperature, x, and q values as shown in Fig. 9(a) ($c=0.8$). The energies of the high density states are significantly reduced as a result of the decrease in the energy penalty on weakened bonds. The differences between the energies of the intermediate- and high-density states are no longer large enough to stabilize low entropy, low energy states and phase transition II does not occur. Based upon the preceding arguments the $L1-L2$ transition should exist for $c=0.3$ if the orientational entropy is sufficiently low (i.e., small q). This is, however, precluded in our study by the lower bound of $q=12$ for the number of distinguishable orientations for a molecule.

Additional mechanisms for the occurrence of polyamorphic transitions exist. In particular, we note an insightful argument by Poole *et al.*[17] regarding the origin of a first-order polyamorphic transition in water, which is based upon results from molecular dynamics simulations of ST2 water. These authors observed, in addition to the usual isothermal minimum in the internal energy as a function of volume, a second, relatively sharp minimum at somewhat larger spe-

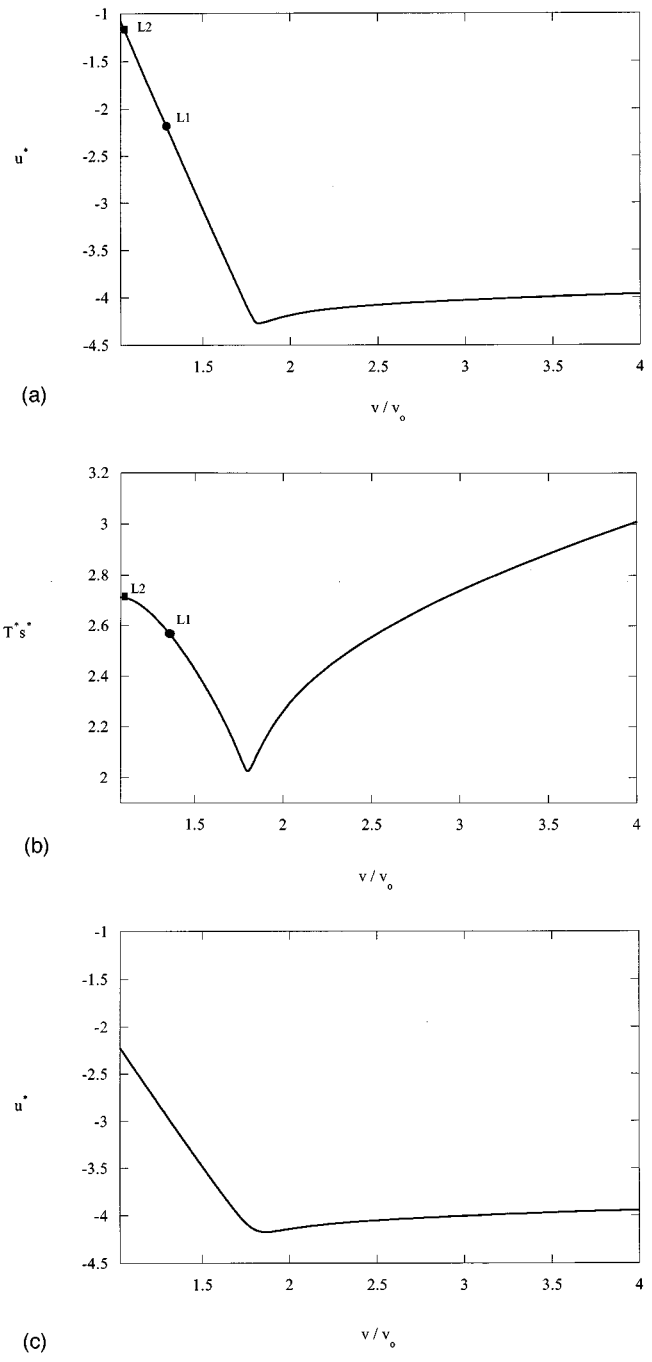

FIG. 9. Reduced, configurational energy ($u^*=U/MJ$) and entropy ($T^*s^*=TS/MJ$) as functions of specific volume, v/v_0 for $T^*=0.15$, $x=0.2$, $q=24$, $c=0.8$ (a),(b) and $c=0.3$ (c). v is the volume per molecule and v_0 is the volume per site. Specific volumes of the equilibrium $L1$ and $L2$ phases in (a) and (b) are indicated by ● and ■, respectively.

cific volumes. This corresponds to the cooperative formation of a random network of hydrogen bonds over a relatively narrow of range of densities. These authors reasoned that because $A \rightarrow U$ as $T \rightarrow 0$, the additional minimum in energy can drive a second fluid–fluid phase transition at low enough temperatures, since this would result in a double-welled $A(v)$ function. The plausibility of this argument was confirmed[17] by solutions to a modified van der Waals equation of state, which showed a second fluid–fluid transition at high pressures and low temperatures. The modification consisted of a bonding interaction which contributed to the energy over a relatively narrow range of fluid densities, giving it a second minimum in its internal energy.

The origins of the second fluid–fluid transition predicted by our model are markedly different from those mentioned above. In our model, transition II occurs because orientational entropy stabilizes the high-density phase. In the results of Poole *et al.*,[17] the second phase transition occurs because energy stabilizes the low-density phase. In terms of phase behavior, the most notable difference which arises from these different scenarios is that the energetic stabilization of the phase transition results in an open-loop two phase region (no LCT), while entropic stabilization of the phase transition gives rise to closed-loop phase behavior.

VI. CONCLUSIONS

We have presented approximate solutions to a lattice model of network fluids that shows polyamorphic behavior at high pressure and low temperature, and exhibits density anomalies over large portions of the liquid phase diagram. Depending upon the relative strengths of the bonding and nonbonding interactions, and the number of possible molecular orientations, both the retracing-liquid-spinodal and the retracing-TMD scenarios are predicted in the mean-field approximation. This confirms earlier findings[15–17] that the different scenarios used to explain the anomalous properties of supercooled water can arise from the same type of molecular interactions. The first-order solution shows two apparently disconnected loci of density extrema. One begins as density maxima in the stable liquid at high pressure, reaches a maximum temperature, and retraces to lower temperature with decreasing pressure; at still lower temperatures this locus becomes a locus of density minima, reverting finally to a locus of density maxima as $T \rightarrow 0$ K. This does not correspond to the known behaviors of classic network fluids such as silica or water, which show only density maxima. The other locus exists only in the region where the liquid is metastable with respect to the vapor. It is always a locus of density maxima, and it terminates at its intersection with the spinodal of the liquid relative to the vapor; which causes the spinodal to retrace to higher pressures at lower temperatures. The large differences between the results obtained by the two methods show that for systems in which molecular orientations are important, the zeroth-order approximation is not sufficient to represent complex fluid behavior and properties; particularly low temperature polyamorphic transitions.

In general, polyamorphism refers to systems with glassy states that differ in density and network topology (e.g., coordination number). The predictions of our model are for equilibrium liquid–liquid transitions, rather than nonergodic, glassy states. Our results remain relevant to the general problem of polyamorphism, however, in light of the apparently first-order LDA-HDA transition, and the questions this raises as to how such a transition would manifest itself if it occurred at temperatures above T_g for the amorphous phases. It

should also be noted that amorphous solid phases are in general metastable with respect to their crystalline phase (s). This topic is not addressed in the present work, as ordered phases were not included in the solutions of the model. The metastability of the liquid phases with respect to ordered phases will be addressed in future work.

Previously, theoretical treatments of network-forming fluids which predict polyamorphic transitions have been restricted to models which assume bulk-density-dependent bonding.[15,17,18] Polyamorphism also arises in ''two-state'' models, in which molecules are assumed to exist in one of two distinguishable states. The first-order solution of our model shows that polyamorphic transitions occur for solutions of the partition function which use only the microscopic interactions described by the fluid's Hamiltonian. For our model, the second fluid–fluid transition arises from a competition between high density states stabilized by the orientational entropy of unbonded molecules, and low density states stabilized by molecules in low-energy, open, fully bonded states.

An estimation of the accuracy of our results is difficult at this stage, because the level of approximation inherent in the first-order solution is quite large for highly bonded states in a network fluid. This derives from the independence of cells in the QC formulation, which neglects fully bonded structures that extend beyond the first coordination shell. The effects of this approximation on the high density phase behavior are difficult to assess. Both the energy and the entropy of the fluid are overestimated, leaving the net effect on the free energy unknown. Improvements which we are presently addressing include applying a mean-field treatment to molecules on the corner sites, expanding the size of the fundamental cell, and obtaining exact solutions from Monte Carlo simulations.

Finally, we wish to emphasize the pronounced differences between the zeroth- and first-order solutions of our model. The dramatic changes in the phase behavior and density anomalies which occur between the two levels of approximation are indicative of the strong influence of states in which the molecules are multiply bonded. Even within the first-order approximation, structures with extended bonding are not considered. The errors which this induces are expected to be significant at the low temperatures and high pressures in which we are interested. In light of the changes caused only by improving the description of the cooperative nature of bond formation in the first-neighbor shell, there is an obvious need for more exact solutions, such as those mentioned above.

ACKNOWLEDGMENTS

C.J.R. would like to thank the National Science Foundation for a Graduate Fellowship. P.G.D. gratefully acknowledges the financial support of the U.S. Department of Energy, Division of Chemical Sciences, Office of Basic Energy Research (Grant No. DE-FG02-87ER13714).

APPENDIX A: MAXIMUM NUMBER OF FLUID–FLUID PHASE TRANSITIONS FROM THE MEAN-FIELD EQUATION OF STATE

We begin by considering the equation of state of the general form $P^*(\rho,T^*)$. We seek solutions which represent two fluid–fluid phase transitions (i.e., a stable vapor–liquid transition, and a liquid–liquid transition which would be metastable with respect to the solid, if the solid was included in the analysis) with meaningful values of ρ, T^*, and the model parameters (x,c,q). A convenient way of casting this problem is to ask if any $P^*-\rho$ projections of the phase diagram show two van der Waals loops. Mathematically this is equivalent to solving

$$\left(\frac{\partial P^*}{\partial \rho}\right)_{T^*}=0 \tag{A1}$$

and seeking sets of (x,c,q) which permit four roots of Eq. (A1). Doing this for Eq. (16) with Eq. (17) yields

$$3A\rho^3-(3A+2B)\rho^2+2B\rho-T^*=0, \tag{A2}$$

where we have used $A\equiv(8x+24\delta J^*)c^*$ and $B\equiv 4(x+3\delta J^*)$. This equation has at most three real, positive roots which implies that $P^*(\rho,T^*)$ cannot have four turning points for a given isotherm. Two van der Waals loops are not possible, and we conclude that the mean-field equation of state is not able to predict a second fluid–fluid phase transition for the present model.

APPENDIX B: MEAN-FIELD APPROXIMATION APPLIED TO THE POTTS VARIABLES

We first rewrite the exponent in Eq. (9) as

$$\beta\left(\frac{J}{3}(1-c)\sum_{\langle ij\rangle} n_i n_j \delta_{ij}+\frac{cJ}{3}\sum_{\langle ij\rangle}^{*}\sum_{k(ij)} n_i n_j \delta_{ij}(1-n_k)\right). \tag{B1}$$

Using this in Eq. (9) and defining $J_1\equiv(J/3)(1-c)$ and $J_2\equiv(cJ/3)$ we then write

$$\sum_{\{\sigma_i\}}\cdots\equiv\sum_{\{\sigma_i\}} Q_b$$

$$=\sum_{\{\sigma_i\}} e^{\beta J_1\Sigma_{\langle ij\rangle}n_i n_j\delta_{ij}} e^{\beta J_2\Sigma_{\langle ij\rangle}\Sigma_{k(ij)}n_i n_j\delta_{ij}(1-n_k)}. \tag{B2}$$

This can be expressed equivalently as

$$\sum_{\{\sigma_i\}}\cdots=\sum_{\{\sigma_i\}}\Pi_{\langle ij\rangle}(1+h_1 n_i n_j\delta_{ij})\Pi_{\langle ij\rangle}\Pi_{k(ij)}(1+h_2 n_i n_j\delta_{ij}(1-n_k)), \tag{B3}$$

with

$$h_1\equiv e^{\beta J_1}-1,$$

$$h_2\equiv e^{\beta J_2}-1.$$

Expanding the products of exponentials, and collecting terms of similar order in $n_i n_j$ gives

$$\sum_{\{\sigma_i\}} \cdots = \sum_{\{\sigma_i\}} \left(1 + h_1 \sum_{\langle ij \rangle} n_i n_j \delta_{ij} + h_2 \sum_{\langle ij \rangle} \sum_{k(ij)} n_i n_j \delta_{ij} (1 - n_k) + \cdots \right). \tag{B4}$$

Now we take terms of order less than or equal to one in $n_i n_j$ and write

$$\sum_{\{\sigma_i\}} \cdots \approx \sum_{\{\sigma_i\}} \left(1 + h_1 \sum_{\langle ij \rangle} n_i n_j \delta_{ij} + h_2 \sum_{\langle ij \rangle} \sum_{k(ij)} n_i n_j \delta_{ij} (1 - n_k) \right). \tag{B5}$$

This is the first-order random-graph approximation proposed by Vause and Walker;[19] the approximation improves as temperature increases, i.e., as h_1 and h_2 become much less than one. The ''sphericallization'' technique treats the remaining summation over $\{\sigma_i\}$. The argument is as follows. For a given distribution of $M(=\Sigma_i n_i)$ molecules on the lattice, there are $q^{\Sigma_i n_i}$ different configurations (q possible orientations for each molecule). Consider two nearest-neighbor molecules within any of these configurations. Within the single-graph or first-order random-graph approximation, the probability of these two molecules being properly oriented for bonding (neglecting any biasing due to favorable energies of specific orientations) is p_b. Thus only p_b of the terms in the summations in Eq. (B5) have δ_{ij} not equal to zero. We can then write

$$\sum_{\{\sigma_i\}} \cdots \approx q^{\Sigma_i n_i} \left(1 + p_b h_1 \sum_{\langle ij \rangle} n_i n_j + p_b h_2 \sum_{\langle ij \rangle} \sum_{k(ij)} n_i n_j (1 - n_k) \right), \tag{B6}$$

which depends upon only $\{n_i\}$. Finally, it is convenient to define an effective bonding interaction energy

$$\delta \mathscr{H} \equiv -\delta J_1 \sum_{\langle ij \rangle} n_i n_j - \delta J_2 \sum_{\langle ij \rangle} \sum_{k(ij)} n_i n_j (1 - n_k), \tag{B7}$$

which defines δJ_1 and δJ_2. Taking $e^{-\beta \delta \mathscr{H}}$ and performing the same random graph approximation as above,

$$\begin{aligned} e^{-\beta \delta \mathscr{H}} &\approx 1 + \delta h_1 \sum_{\langle ij \rangle} n_i n_j + \delta h_2 \sum_{\langle ij \rangle} \sum_{k(ij)} n_i n_j (1 - n_k), \\ \delta h_1 &= e^{\delta J_1} - 1, \\ \delta h_2 &= e^{\delta J_2} - 1. \end{aligned} \tag{B8}$$

Multiplying by $q^{\Sigma_i n_i}$, equating the resultant expression to $\Sigma_{\{\sigma_i\}} \cdots$, and comparing like terms gives

$$\begin{aligned} \delta J_1 &= kT \ln(1 + p_b(e^{\beta J_1} - 1)), \\ \delta J_2 &= kT \ln(1 + p_b(e^{\beta J_2} - 1)). \end{aligned}$$

Finally, we define

$$\delta J \equiv \delta J_1 / 3 + \delta J_2 \tag{B9}$$

and

$$c^* \equiv \frac{\delta J_2}{\delta J_1} \left(\frac{1}{3} + \frac{\delta J_2}{\delta J_1} \right)^{-1}. \tag{B10}$$

Substituting into Eqs. (B3) to (B5) yields

$$\Xi(\mu, V, T) \approx \sum_{n_i} e^{(\beta \mu + \ln q) \Sigma_j n_j} e^{\beta \epsilon \Sigma_{\langle ij \rangle} n_i n_j} e^{\beta \delta J \Sigma^*_{\langle ij \rangle} n_i n_j \Sigma_{k(ij)} (1 - c^* n_k)}, \tag{B11}$$

which is Eq. (10).

APPENDIX C: ADDITIONAL DETAILS OF THE DERIVATION OF THE QC EQUATION OF STATE

Writing Eqs. (23) and (24) explicitly in terms of ψ_c and ψ_d we have

$$\rho = \frac{1}{\alpha} \left(\sum_j^* \psi_j \omega_j n_j + \psi_c \omega_c n_c + \psi_d \omega_d n_d \right), \tag{C1}$$

$$(1 - \rho) = \frac{1}{\alpha} \left(\sum_j^* \psi_j \omega_j (\alpha - n_j) + \psi_c \omega_c (\alpha - n_c) + \psi_d \omega_d (\alpha - n_d) \right). \tag{C2}$$

In the above expressions, the superscript * is to indicate that the summations do not include cell configurations c and d. Equations (C1) and (C2) can be rearranged to allow us to write expressions for ψ_c and ψ_d:

$$\psi_c = \frac{1}{\omega_c (n_c - n_d)} \left[\alpha \rho - \sum_j^* \omega_j \psi_j n_j - n_d \left(1 - \sum_j^* \omega_j \psi_j \right) \right], \tag{C3}$$

$$\psi_d = \frac{1}{\omega_d (n_c - n_d)} \left[-\alpha \rho + \sum_j^* \omega_j \psi_j n_j + n_c \left(1 - \sum_j^* \omega_j \psi_j \right) \right]. \tag{C4}$$

This shows that the cell configurations c and d cannot be chosen arbitrarily. They must be such that $n_c \neq n_d$, otherwise Equations (C3) and (C4) are no longer independent.

Using Eq. (27), and since ψ_c and ψ_d are functions of ρ, we have

$$P v_0 = \rho \left[\left(\frac{\partial a}{\partial \rho} \right)_{T, \{\psi_j\}} + \left(\frac{\partial a}{\partial \psi_c} \right) \left(\frac{\partial \psi_c}{\partial \rho} \right) + \left(\frac{\partial a}{\partial \psi_d} \right) \left(\frac{\partial \psi_d}{\partial \rho} \right) \right] - a. \tag{C5}$$

Expressions for the partial derivatives in Equation (C5) are obtained from Eq. (27)

$$\left(\frac{\partial a}{\partial \psi_c} \right) = \frac{\omega_c}{2} (\epsilon_c + kT(1 + \ln \psi_c)), \tag{C6}$$

$$\left(\frac{\partial a}{\partial \psi_d} \right) = \frac{\omega_d}{2} (\epsilon_d + kT(1 + \ln \psi_d)), \tag{C7}$$

and

$$\left(\frac{\partial a}{\partial \rho}\right)_{T,\{\psi_j\}} = -\frac{kT}{2}\sum_{j=1}^{m}\omega_j\left(\frac{\partial \psi_j^{\infty}}{\partial \rho}\right)_{T,\{\psi_j\}}(1+\ln\,\psi_j^{\infty}) + kT\ln\frac{\rho}{q(1-\rho)}\,. \tag{C8}$$

And from Table I we see that

$$\psi_j^{\infty} = \left(\frac{\rho}{q}\right)^{n_j}(1-\rho)^{9-n_j}, \quad j=1,2,\ldots,c,\ldots d,\ldots m.$$

From Eqs. (C3) and (C4) we can write

$$\left(\frac{\partial \psi_c}{\partial \rho}\right) = \frac{9}{\omega_c(n_c-n_d)}, \tag{C9}$$

$$\left(\frac{\partial \psi_d}{\partial \rho}\right) = -\frac{9}{\omega_d(n_c-n_d)}. \tag{C10}$$

Equation (29) follows from Eqs. (C5) and (C6)–(C10)

Referring now to the expression for (ψ_j/ψ_c), Eq. (32) follows from

$$\left(\frac{\partial a}{\partial \psi_j}\right)_{T,\rho,\{\psi_j\}_{j\neq c,d}} = \left(\frac{\partial a}{\partial \psi_j}\right)_{T,\rho,\{\psi_{k\neq j}\}} + \left(\frac{\partial a}{\partial \psi_c}\right)\left(\frac{\partial \psi_c}{\partial \psi_j}\right) + \left(\frac{\partial a}{\partial \psi_d}\right)\left(\frac{\partial \psi_d}{\partial \psi_j}\right) = 0 \tag{C11}$$

in conjunction with Eqs. (27), (C3), and (C4).

[1] F. Sciortino, P. H. Poole, H. E. Stanley, and S. Havlin, Phys. Rev. Lett. **64**, 1686 (1990).
[2] R. L. Blumberg and H. E. Stanley, J. Chem. Phys. **80**, 5230 (1984).
[3] F. H. Stillinger, Science **209**, 451 (1980).
[4] R. G. Della Valle and H. C. Andersen, J. Chem. Phys. **97**, 2682 (1992).
[5] C. A. Angell, Science **267**, 1924 (1995).
[6] C. A. Angell, Annu. Rev. Phys. Chem. **34**, 593 (1983).
[7] M. Grimsditch, Phys. Rev. Lett. **52**, 2379 (1984).
[8] O. Mishima, J. Chem. Phys. **100**, 5910 (1994).
[9] C. A. Angell, P. H. Poole, and J. Shao, Nuovo Cimento **16D**, 993 (1994); The term polyamorphism has been suggested [G. H. Wolf, S. Wang, C. A. Herbst, D. J. Durben, W. J. Oliver, and Z. C. Halvorsen, in *High Pressure Research: Application to Earth and Planetary Sciences*, edited by Y. S. Manghnani and M. H. Manghnani (Terra Sci. Publ. Co./Am. Geophysical Union, Tokyo/Washington, 1992), p. 503] for the coexistence of amorphous phases having the same composition but different density and structure.
[10] O. Mishima, L. D. Calvert, and E. Whalley, Nature **314**, 76 (1985).
[11] O. Mishima, L. D. Calvert, and E. Whalley, Nature **310**, 393 (1984).
[12] A notable exception to this, which provides support for the use of density-driven polyamorphism to infer a liquid–liquid transition above T_g, is the recent experimental work of S. Aasland and P. F. McMillan [Nature **369**, 633 (1994)].
[13] E. G. Ponyatovsky and O. I. Barkalov, Mat. Sci. Rep. **8**, 147 (1992).
[14] G. M. Bell, J. Phys. C: Solid State Phys. **5**, 889 (1972); G. M. Bell and D. W. Salt, Trans. Faraday Soc. II **72**, 76 (1975); P. H. E. Meijer, R. Kikuchi, and P. Papon, Physica A **109**, 365 (1981); P. H. E. Meijer, R. Kikuchi, and E. van Royen, Physica A **115**, 124 (1982); M. Sasai, Bull. Chem. Soc. Jpn. **66**, 3362 (1993); N. A. M. Besseling and J. Lyklema, J. Phys. Chem. **98**, 11610 (1994).
[15] S. S. Borick, P. G. Debenedetti, and S. Sastry, J. Phys. Chem. **99**, 3781 (1995).
[16] S. Sastry, F. Sciortino, and H. E. Stanley, J. Chem. Phys. **98**, 9863 (1993).
[17] P. H. Poole, F. Sciortino, T. Grande, H. E. Stanley, and C. A. Angell, Phys. Rev. Lett. **73**, 1632 (1994).
[18] E. G. Ponyatovskii, V. V. Sinand, and T. A. Pozdnyakova, JETP Lett. **60**, 360 (1994).
[19] C. A. Vause and J. S. Walker, Phys. Lett. A **90**, 419 (1982).
[20] P. G. Debenedetti, V. S. Raghavan, and S. S. Borick, J. Phys. Chem. **95**, 4540 (1991).
[21] R. J. Speedy, J. Phys. Chem. **86**, 982 (1982).
[22] P. H. Poole, F. Sciortino, U. Essmann, and H. E. Stanley, Nature **360**, 324 (1992).